Dielectric Properties of C_{60} and $Sc_3N@C_{80}$ Fullerenol Containing Polyurethane Nanocomposites

Hanaa M. Ahmed,[1] Mohammad K. Hassan,[2,3] Kenneth A. Mauritz,[2] Steven L. Bunkley,[4] Randy K. Buchanan,[4] J. Paige Buchanan[1]

[1]Department of Chemistry and Biochemistry, University of Southern Mississippi, Hattiesburg, Mississippi 39406
[2]School of Polymers and High Performance Materials, University of Southern Mississippi, Hattiesburg, Mississippi 39406
[3]Department of Chemistry, Faculty of Science, Bani Suef University, Bani Suef, Egypt
[4]School of Computing, University of Southern Mississippi, Hattiesburg, Mississippi 39406
Correspondence to: J. P. Buchanan (E-mail: paige.buchanan@usm.edu)

ABSTRACT: Polymer–fullerene nanocomposites consisting of linear polyurethane (PU) chains crosslinked via increasing loadings of polyhydroxylated fullerenes (C_{60} and $Sc_3N@C_{80}$, a metallic nitride fullerene) were prepared and characterized for their mechanical and dielectric properties using dynamic mechanical analysis (DMA) and broadband dielectric spectroscopy (BDS). Fullerene–polymer networks [C_{60}-PU and $Sc_3N@C_{80}$-PU] having high gel fractions, good mechanical properties and thermal stabilities were produced. Polyhydroxylated fullerenes $C_{60}(OH)_{29}$ and $Sc_3N@C_{80}(OH)_{18}$ were synthesized in high yield through a high-speed vibration milling method and characterized using FTIR, matrix-assisted laser desorption/ionization mass spectroscopy, and thermal gravimetric analysis. DMA of fullerene–PU networks indicates $T_g \sim -50°C$, with a sub-T_g relaxation due to local chain motions. BDS analyses of the fullerenes, before and after hydroxylation and before incorporation into the networks, revealed one relaxation and large real permittivity (ε') values for $C_{60}(OH)_{29}$ relative to C_{60}. Analogous samples for $Sc_3N@C_{80}$ exhibit two relaxations, where the extra relaxation is attributed to motions of the cage-encapsulated Sc_3N clusters. ε' values for $Sc_3N@C_{80}$-PU at a given frequency are higher than corresponding values for C_{60}-PU, likely because of the rotationally mobile Sc_3N encapsulates. Surface and bulk resistivities of fullerene–PU networks were found to have a modest dependence on relative humidity. Capacitance versus voltage characteristics of the fullerene–PUs were also studied in the range of the applied dc bias voltage of -30 to $+30$ v. It is generally concluded, based on all the evidence that this class of materials can be rendered quite polarizable and could be used as high dielectric permittivity materials in capacitance applications. © 2014 Wiley Periodicals, Inc. J. Appl. Polym. Sci. **2014**, *131*, 40577.

INTRODUCTION

Encapsulation of metal atoms inside fullerene cages, forming endohedral metallofullerenes, significantly alters the fullerene electronic structure and produces novel materials, which hold promise in applications of charge separation, transport, and storage.[1–4] Metallic nitride fullerenes (MNF), a relatively new class of metallofullerene compounds, possess a metal-nitride cluster (M_3N) encapsulated within the fullerene cage.[5,6] An interesting feature of MNFs, of which $Sc_3N@C_{80}$ is the most stable and abundant member, is the charge transfer from the metal to the carbon shell that has been demonstrated to alter the electronic and magnetic properties of MNF fullerenes.[7–10] Allowing for the incorporation of metals having magnetic, electroactive,

and radioactive properties, MNFs are expected to show promising performance as substituent materials in the diverse application areas of electronics,[11] optical,[12] and biological.[13,14]

Our interest lies in the combination of the exciting characteristics of MNFs with the processability of polymers, that is, polymeric materials are intrinsically considered as useful scaffolds for the construction of high molecular weight structures. Therefore, this combination would, in principle, yield advanced, high-performance materials with potential applications in superconductors, lasers, ferroelectrics, and so on.[15] C_{60} fullerene containing-polymers have received much attention in recent years due to their unusual properties and anticipated applications.[16–22] An interesting feature of these C_{60}-polymer

Additional Supporting Information may be found in the online version of this article.

nanocomposites lies in the possibility of tuning the mechanical properties of the composite through modification of the chemical linkages among the matrix constituents. Although several studies are reported on C_{60}-polymer nanocomposites, few studies exist concerning the metallofullerene-analogs.[23–25] One example of these studies reports the stimuli-responsive adhesive properties of the blends of $Sc_3N@C_{80}$ and polystyrene-*block*-polyisoprene-*block*-polystyrene (SIS) copolymer.[25]

A number of techniques can be used to investigate the properties of polymer nanocomposites. A lesser used method is dielectric spectroscopy which addresses molecular dynamics and electrical polarizability.[26] A dielectric response results from the interaction of dipoles or polarizable elements with an applied electric field that oscillates at different frequencies (f) at given temperatures. The essential quantity is the complex dielectric permittivity which is given by eq. (1)[27]:

$$\varepsilon*(\omega) = \varepsilon'(\omega) - i\varepsilon''(\omega) \tag{1}$$

ω is the angular frequency $= 2\pi f$ and $i = \sqrt{-1}$. ε', the real permittivity, reflects material polarizability that can be due to dipole reorientation, deformation of delocalized electron distributions or interfacial polarization (internal or sample/electrode). ε'', the imaginary, or loss permittivity, is proportional to the energy dissipated per cycle during any of these processes, termed 'relaxations'. Modern broadband dielectric spectroscopy (BDS) is a very powerful tool for probing the molecular dynamics of polymers because the system can be analyzed over a broad frequency range that usually extends from the milli- to megahertz region.[26] Therefore, motional processes which take place in polymers on extremely different time scales, or relaxation times, can be investigated versus temperature.

Numerous exciting properties of metallofullerenes result from the encapsulated metals, for example, optical (Er), magnetic (Gd), radioactive (Ho); however, few studies of their dielectric properties are found in the literature. Iwasa et al.[28] related the dielectric properties of a $La@C_{82}$ solid to their molecular motions, and the temperature dependence of these properties revealed that the metallofullerenes are dielectrically active due to the rotational mobility of their encapsulated dipoles. Herein we report, for the first time, the preparation and characterization of $Sc_3N@C_{80}$-containing polyurethane (PU) nanocomposites. The essential characterizations of these nanocomposites involved probing their thermal stability, mechanical, and dielectric properties.

EXPERIMENTAL

Materials
Materials used for the hydroxylation of fullerenes are C_{60} (MER, 99+%), toluene (Aldrich, 99.9%), potassium hydroxide (Aldrich, 85+%), and Sephadex G-25 (Aldrich, dry head diameter of 20–80 μm and bed volume of 4–6 mL/g). $Sc_3N@Ih\text{-}C_{80}$ (>99%) used in this study was purified from commercial samples (SES) according to previous work.[5,6]

Materials used for the preparation of fullerene–PU networks were methylenebis (4-isocyanatobenzene) (MDI, 98%) and methanol (99.8%, HPLC grade) purchased from Sigma Aldrich.

Poly(tetramethylene oxide) glycol (PTMO, $M_n = 2000$) was purchased from Monomer-Polymer & Dajac Labs. N,N-Dimethylorformamide (DMF, 99.9%) and tetrahydrofuran (THF, 99.9%) were purchased from Fisher. All solvents were dried before use: THF was distilled over sodium, and DMF was dried over 4 Å molecular sieves. Unless otherwise noted, all commercial materials were used as received without further purification.

Preparation of Hydroxylated $C_{60}(OH)_x$ and $Sc_3N@C_{80}(OH)_y$
The hydroxylation of C_{60} and $Sc_3N@C_{80}$ was performed under high-speed vibration milling conditions in which 0.062 mmol of fullerene and 16 mmol KOH were charged to a stainless steel capsule along with three stainless steel milling balls. The capsule was vigorously shaken, for 1 h in the case of C_{60} and 7 h for $Sc_3N@C_{80}$, using a milling machine (Spex mixer/miller 8000) at room temperature. The solid reaction mixture was then added to 5 mL of deionized water, yielding a brown homogenous solution. The crude solution was filtered through a 0.5-μm PTFE membrane, and water was partially removed under reduced pressure. The concentrated crude sample was chromatographed on a Sephadex G-25 size-exclusion gel column with distilled water as the eluent, thereby removing residual salts. Furthermore, to obtain final fullerenols with a narrow distribution range of hydroxyl number, the sample was collected (pH 6–7) as a dark brown solution over a short time interval. The collected sample was concentrated under reduced pressure and added dropwise to 100 mL of methanol to produce a precipitate of brown solids. The precipitate was separated by filtration through a 47-mm 0.2-μm PTFE membrane, followed by drying at 50°C under vacuum to give $C_{60}(OH)_x$ and $Sc_3N@C_{80}(OH)_y$ in isolated yields of ~83 and 65%, respectively. The purified hydroxylated fullerenes were characterized by FTIR spectroscopy, thermal gravimetric analysis (TGA), and matrix-assisted laser desorption/ionization mass spectroscopy (MALDI-MS).

Preparation of C_{60}-PU and $Sc_3N@C_{80}$-PU Films
In a typical preparation, a three-necked reaction vessel (25 mL) was charged with MDI (2.1 equiv.), PTMO (1 equiv.), and THF. The reaction mixture was stirred at 60°C under nitrogen for 10 h producing diisocyanate end-capped prepolymer. At the completion of this step and in the same reaction vessel, an appropriate amount of fullerenol, $C_{60}(OH)_x$ or $Sc_3N@C_{80}$ $(OH)_y$ (dried under vacuum at 60°C for 24 h and ultrasonicated in a small amount of dry DMF for 1 h to suspend), was stirred with the prepolymer in a mixture of THF and DMF (3 : 1) at 60°C under nitrogen for 16 h. Within 5 h, the reaction mixture became more viscous. After 16 h, the viscous solution was poured into an evaporating dish, and the solvent was slowly evaporated under N_2 to afford a pliable film. The film was removed from the mold and suspended in methanol, while sonicated briefly at room temperature to quench unreacted prepolymer. Removal of methanol and drying at 60°C under vacuum yielded fullerene-crosslinked PU networks. Two series of fullerene–PU networks were prepared: C_{60}-PU and $Sc_3N@C_{80}$-PU at four different loadings of fullerene 0.8, 1, 2, and 3% (w/w).

Instrumentation and Characterization Methods
FTIR and Gel Fraction. The infrared spectra of the prepared samples were recorded in the wavenumber range of 400–4000 cm^{-1}

using a Nicolet Nexus 470 FTIR spectrometer. Gel fractions of prepared films were obtained by dissolving a known mass of film in chloroform, resting the sample for 24 h at room temperature, and recovering the insoluble mass fraction, followed by residual solvent evaporation under reduced pressure. The gel fraction is the final mass after extraction over the initial mass, reflected as a percent.

Matrix-Assisted Laser Desorption/Ionization Mass Spectroscopy. The mass spectra of the hydroxylated fullerene were collected using MicroFlex Bruker Daltonics mass spectrometer, applying flexControl method with a laser power ranging from 30 to 55. For MALDI mass spectroscopy, 1,8,9-anthracenetriol (MW of 226.23) dissolved in acetonitrile at a concentration of 5 mg in 500 μL was used as a matrix. A small amount of the hydroxylated fullerenes, dissolved in water, was mixed with the matrix solution and then applied to the target plate via syringe, followed by solvent evaporation under a nitrogen stream. Pure samples of C_{60} (FW = 720.67 g/mol) and $Sc_3N@C_{80}$ (FW = 1109 g/mol) were dissolved, individually, in toluene and used as references.

Thermal Gravimetric Analysis. The thermal stability of the prepared networks was evaluated by TGA, where weight changes in a material are monitored as a function of temperature under a controlled atmosphere. Using a TA instruments Q5000, average 10 mg samples were analyzed in platinum pans over the temperature range of 25–1000°C at a heating rate of 20°C/min. The number of hydroxyl groups attached to the fullerene cage was estimated by calculating the ratio of the weight loss at 250°C, corresponding to the sample dehydroxylation, to the weight loss at temperature >300°C. For fullerene–PU networks, the thermal degradation onset temperature was reported as the temperature corresponding to 10% mass loss.

Dynamic Mechanical Analysis. The dynamic storage modulus (E') as well as tan $\delta = E''/E'$ were measured using a dynamic mechanical analysis (DMA) Thermal Analysis Q800 instrument. All samples were run in tensile mode with a frequency of 1 Hz and an amplitude of 15 μm. The experiments were performed over the temperature range −150 to 100°C at a heating rate of 2°C/min.

Dielectric Measurements. Dielectric measurements on fullerene–PU films were performed using a Novocontrol. Concept 80 broadband dielectric spectrometer, and data were collected over the frequency range 0.1 Hz to 3 MHz at fixed temperatures in the range of −150 to 180°C. The temperature stability of the instrument was within +/− 0.2°C. Samples were kept in a Humidity Control Chamber (Model 503-20, Electro-tech Systems) with RH <0.5% at room temperature for more than 1 week before analysis. Sample discs of 2 cm diameter that were covered with two very clean aluminum sheets on both sides were sandwiched between two gold-coated copper electrodes of 2 cm diameter and transferred to the instrument for data collection. For powder samples, a Novocontrol BDS 1308 liquid/powder parallel plate sample cell was used. Cell capacity was adjusted by variation of electrode spacing using silica or Teflon spacers.[31]

Dielectric properties were also measured using a Keithley 4200 Semiconductor Characterization System (SCS) connected to a

custom designed parallel plate electrode assembly at room temperature (22°C) under controlled humidity. The assembly contains a circular parallel plate electrode (diameter of 1.25 cm) encased in an electrically grounded box to prevent interference from external sources. The sealed enclosure was designed to maintain a constant humidity through the delivery of a controlled ratio of dry versus wet inert feed gases. Two types of permittivity tests were performed with this assembly. The first test measured permittivity at frequencies spanning a range from 10 kHz to 10 MHz in graduated logarithmic steps with 0 VDC (volts dc) bias. For the second test, the DC offset voltage was swept from −30 to +30 VDC in 1 VDC steps at a constant frequency. Both tests calculated capacitance by measuring the root mean squared (rms) current at the given frequency and rms voltage. The standard equations for parallel plate capacitor geometry were used to calculate permittivity from the measured capacitance.

Resistivity Measurements. The Keithley 4200-SCS and the custom assembly was also used to measure surface and volumetric resistivity over a voltage range of −210 to +210 VDC in 1 VDC steps. Modifications were made to the custom assembly relative to the electrode design to allow switching between surface and volumetric resistivity tests as per ASTM D257-07. The bottom electrode was comprised of two separate electrodes, an inner and an outer ring. Volumetric measurements were acquired by applying a potential between the top and bottom inner electrode plates, allowing current to flow through the material. Surface measurements were acquired by applying a potential between the bottom inner and outer ring electrodes. The unused electrode in both configurations was disconnected from source and ground. Calculations involving surface and volumetric resistivity were performed according to the previously stated ASTM standard.

RESULTS AND DISCUSSION

The general synthesis route for the preparation of fullerene–polymer networks, described as fullerene–PU, includes the use of the hydroxylated fullerene as a polyfunctional monomer, $C_{60}(OH)_x$ for C_{60}-PU and $Sc_3N@C_{80}(OH)_y$ for $Sc_3N@C_{80}$-PU, in reactions with linear isocyanate terminated polyether segments according to Scheme 1. In this study, the PTMO and MDI concentration were held constant at 2.1 : 1 (MDI:PTMO) molar equivalents in the preparation of the diisocyanate, end-capped prepolymer. Two different sets of fullerene–PU networks were prepared, each set with increasing fullerene content from 0.8 to 3% (w/w). Sample identifiers and the corresponding OH:NCO molar ratios are reported in Table I.

Characterization of fullerenols ($C_{60}(OH)_x$ and $Sc_3N@C_{80}(OH)_y$) was afforded through a number of standard techniques.[29] FTIR data collected on vacuum dried samples support the attachment of hydroxyl groups (3500 cm^{-1}) to the carbon cage of both C_{60} and $Sc_3N@C_{80}$. Also, these spectra presented three characteristic bands at 1080, 1370, and 1620 cm^{-1} assigned to vC-O, δ_sC-O-H and vC=C absorptions. These four broad bands are invariably reported as diagnostic absorptions of various fullerenols.[30,31] TGA can be a valuable means to elucidate chemical structure,
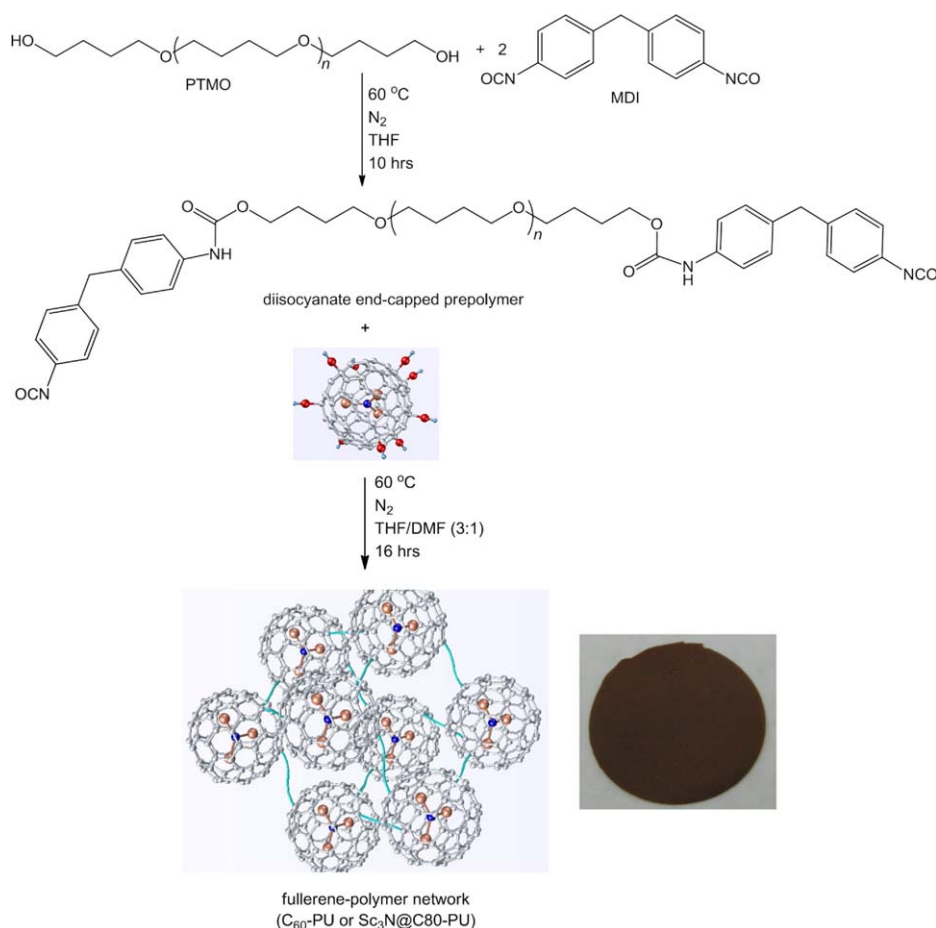
Scheme 1. Preparation of fullerene–PU network. [Color figure can be viewed in the online issue, which is available at wileyonlinelibrary.com.]

when one functional group has a characteristic thermal decomposition temperature. The mass loss from $C_{60}(OH)_x$ fullerenol samples was monitored and assigned according to methods reported by Yannoni et.al.:[32] RT to 110°C = secondary bound water; 110–300°C = dehydration and subsequent loss of the attached hydroxyl; and >300°C = decomposition of the fullerene nucleus. The number of hydroxyl groups attached are approximated for $C_{60}(OH)_x$ and $Sc_3N@C_{80}(OH)_y$ at 28 and 17 OH, respectively. MALDI-MS analysis on fullerenol samples, referenced to the pure C_{60} and $Sc_3N@C_{80}$ parent compounds and using 1,8,9-anthracenetriol as matrix, yields parent ions at m/z 1230 and 1725, corresponding to $C_{60}(OH)_{30}$ and $Sc_3N@C_{80}(O)_{18}(OH)_{19}$. MS analysis also suggests the presence of $Sc_3N@C_{80}$ oxides, due presumably to incomplete hydroxylation.[33] In all stoichiometric calculations for polymerization reactions, the average values of $C_{60}(OH)_{29}$ and $Sc_3N@C_{80}(OH)_{18}$ are used. Network-forming reactions are monitored by FTIR using the disappearance of the absorption band of the NCO group (at 2272 cm^{-1}) of the prepolymer and the simultaneous appearance of the urethanic NH and carbonyl absorption bands (at 3311 and 1728 cm^{-1}, respectively) of the network. A small absorbance remains at 3500 cm^{-1} in the prepared networks due to potential error in the approximated number of OH groups, incomplete reaction of the end groups, or residual water molecules. The contribution of these residuals is considered in drawing conclusions in the characterization of the networks. This general network-forming approach produces films having good

Table I. Characterization of Fullerene–PU Networks: Gel Fraction and Thermal Stabilities

Sample ID[a]	OH:NCO (equiv)[b]	Gel fraction wt %[c]	Thermal degradation onset (°C)[d]
0.8% C_{60}-PU	1 : 4	72	322
1% C_{60}-PU	1 : 3	97	330
2% C_{60}-PU	1 : 1.5	82	324
3% C_{60}-PU	1 : 1	83	327
0.8% $Sc_3N@C_{80}$-PU	1 : 7	85	343
1% $Sc_3N@C_{80}$-PU	1 : 5	77	330
2% $Sc_3N@C_{80}$-PU	1 : 3	80	331
3% $Sc_3N@C_{80}$-PU	1 : 1.7	85	332

[a] wt % of $C_{60}(OH)_{29}$ or $Sc_3N@C_{80}(OH)_{18}$ in films.
[b] Hydroxyl and isocyanate functional group equivalents.
[c] Insoluble mass fraction recovered after 24-h solvent exposure.
[d] TA Instruments Q5000 TGA parameters, high-resolution method, onset = temperature corresponding to 10% mass loss after water loss.

mechanical properties and thermal stabilities. Gel fractions of the prepared fullerene–PU networks are listed in Table I and are in general high. Information about the thermal stability of the prepared fullerene–PU networks were obtained from TGA techniques, and thermal degradation onsets corresponding to 10% mass loss are reported (selected plots are included in the Supporting Information section).[29] Fullerene–PU networks show no significant weight loss up to 300°C. A correlation of degradation onset to gel fraction is suggested, but all samples are considered to have excellent thermal stability for urethane-containing polymer networks.

Dynamic storage modulus (E') and loss tangent, tan $\delta = E''$ (loss modulus)/E' versus temperature curves for fullerene–PU networks are provided in Figure 1(a,b), respectively. The E' curves depict a glassy material at low temperatures and a rubbery material at high temperatures with a glass transition at approximately $-50°C$ that is associated with the onset of long range chain segmental mobility of the PU fraction. For three compositions—3% C_{60}-PU, 2% C_{60}-PU, and 2% $Sc_3N@C_{80}$— there is a significant and reproducible increase in modulus with increase in temperature in the rubbery state. This increase in modulus is attributed to thermally driven network crosslinks during analysis. Three distinct maxima are observed on the tan δ versus temperature plots. The origin of the peak in the temperature range of -150 to $-110°C$ (observed in all samples) is assigned to crankshaft motions of the methylene sequences in PTMO soft segments, based on earlier work.[34–37] The maximum in the tan δ plots (range of -48 to $-52°C$) corresponds to the most active region of the glass transition at T_g and does not appear to correlate to the composition of the networks. The high temperature shoulder is likely due to the thermally driven reactions described previously.

The nature of the dynamic dielectric properties of $Sc_3N@C_{80}$, $Sc_3N@C_{80}(OH)_{18}$, and $Sc_3N@C_{80}$-PU nanocomposites are presented in comparison to those of C_{60}, $C_{60}(OH)_{29}$, and C_{60}-PU networks. The broad frequency range of 0.1 Hz to 3 MHz over the temperature range -150 to $180°C$ allows for an interrogation of molecular motions and charge displacements related to polarizability over vast time and distance scales.

Figure 2(a,b) illustrates the frequency dependences of ε' for C_{60} and $Sc_3N@C_{80}$ powders at several select temperatures. For both materials, ε' decreases with increasing frequency and the curves are displaced upward with increase in temperature, in the usual fashion. The upward curve displacement is attributed to the freely rotating encapsulate which increases the polarizability and therefore, ε'. The decrease in ε' with increasing f is a consequence of the fact that the time scale during which the electric field is applied in one direction—that is, one-half the period of oscillation $= 1/2f$—decreases with increasing frequency. In essence, faster motions associated with polarizability have less time to be sampled.

The magnitude of ε' across the frequency range observed on C_{60} curves is considerably less than corresponding values on the $Sc_3N@C_{80}$ curves. This is reasonable because C_{60} has spherical symmetry, no polar groups, and the only inherent polarizability is attributed to fluctuations in the distribution of delocalized
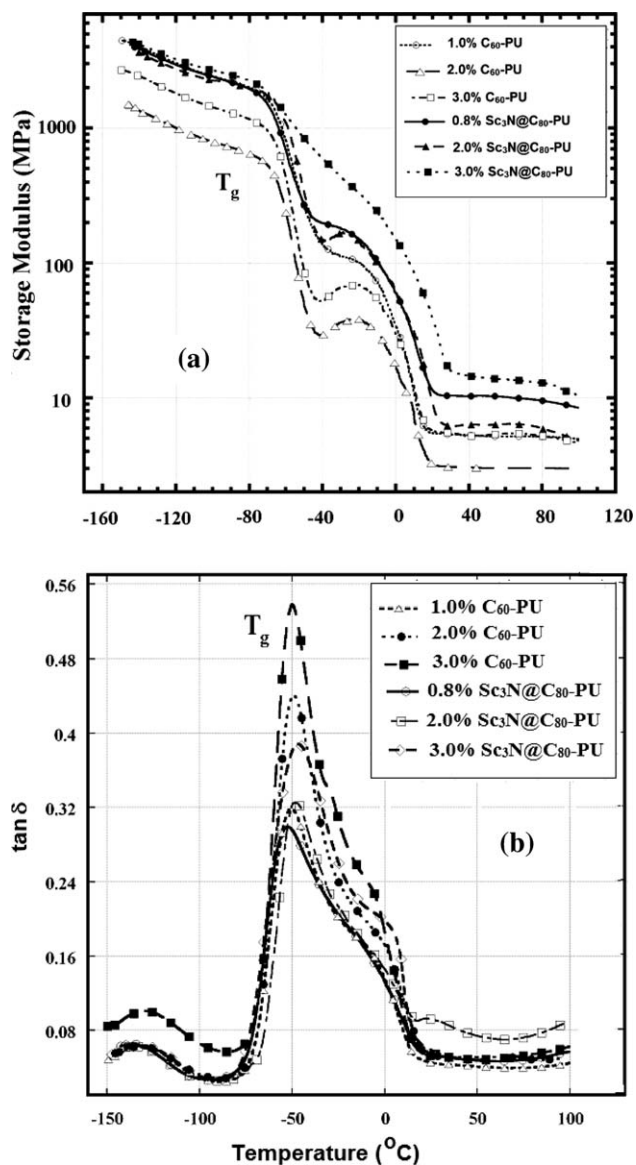
Figure 1. (a) Dynamic storage modulus (E') and (b) loss tangent (tan δ) versus temperature for fullerene–PU compositions.

electrons on the cage. The higher ε' values seen on $Sc_3N@C_{80}$ curves reflect greater polarizability is assigned to a combination of electronic cage distortions, the presence of metals with loosely bound electrons, and a freely rotating polarizable encapsulate. The increase in temperature imparts more freedom of motion to these polarizability contributors, which, in turn, increases ε' at a given temperature and frequency. Relevant to these results are prior studies indicating that solid C_{60} arrays rotate almost freely in a rotationally disordered high-temperature, face-centered cubic phase (above 260 K at atmospheric pressure). This motion is said to slow down and is transformed into a ratcheting or rocking motion in an orientation-ordered simple cubic phase at low temperatures and high pressures.[38–40] Su et al.[38,39] demonstrated a structural phase transition at 260 K as well as an anomaly at 90 K resulting from a glass transition. Furthermore, these investigators observed a Debye-like relaxation in the dielectric response,
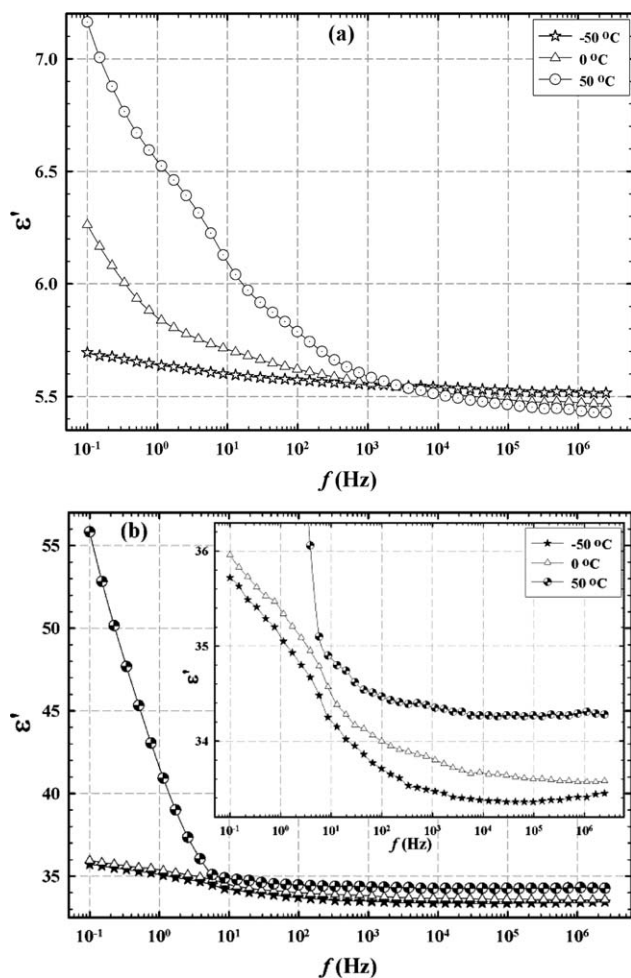
Figure 2. ε' versus frequency for (a) C_{60} and (b) $Sc_3N@C_{80}$ samples at three temperatures.

which suggests the existence of dipole reorientations in microcrystalline C_{60} films.

ε' and tan δ versus f curves at three temperatures for $C_{60}(OH)_{29}$ and $Sc_3N@C_{80}(OH)_{18}$ are provided in Figures 3 and 4, respectively. The monotonically decreasing ε' behavior with increase in f, in both cases, is due to an increasing inability of the natural time scale of the dynamics of polarization to be captured within increasingly smaller signal time scales, that is, decreasing $1/2f$. The magnitude of ε' values for $C_{60}(OH)_{29}$ for a given f and T are much larger when compared to unfunctionalized C_{60}. This increase in dielectric response is attributed to the attachment of the polar OH groups to the cages. It would seem that the only way to achieve these high polarizabilities is for the $C_{60}(OH)_{29}$ particles to rotate. Also, it is unlikely that the hydroxylation is uniform across the C_{60} cage surface, making it impossible for the dipole moments of all the -OH groups to cancel on a given cage.

High real permittivities, ε', observed at low frequencies might be caused in part by sample | electrode interfacial polarization which is not a bulk material phenomenon but the result of blocking electrodes at the sample surfaces. ε' values of

$C_{60}(OH)_{29}$ are much higher than those of $Sc_3N@C_{80}(OH)_{18}$ and this increase is attributed to the larger number of cage-attached OH groups on the latter (29 vs. 18, respectively). In Figure 3(b), ε' is slightly higher at 0°C than at 50°C in the low frequency region, which we attribute to the differences in packing densities of the powder samples. ε' is dependent, in part, on the average dipole moment per unit volume; therefore, slight differences packing density may affect ε'.

Figure 4(a,b) describes the frequency dependence of tan δ at specific temperatures for $C_{60}(OH)_{29}$ and $Sc_3N@C_{80}(OH)_{18}$. With both compositions, and as the temperature increases, the peaks shift to higher frequencies, as more thermal kinetic energy is imparted to polar groups causing greater ease of reorientation. Tan δ values for $C_{60}(OH)_{29}$ are larger than those of $Sc_3N@C_{80}(OH)_{18}$ owing again to the higher degree of hydroxylation of the former. Interestingly, the curves for $Sc_3N@C_{80}(OH)_{18}$ are more complex in that there are two relaxation peaks on each spectrum. A possible explanation is that one peak is due to cage reorientation while the other is due to tumbling motions of the Sc_3N encapsulated in the cage. A separate manuscript is in preparation—applying additional theoretical treatments—to address the subtleties concerning the
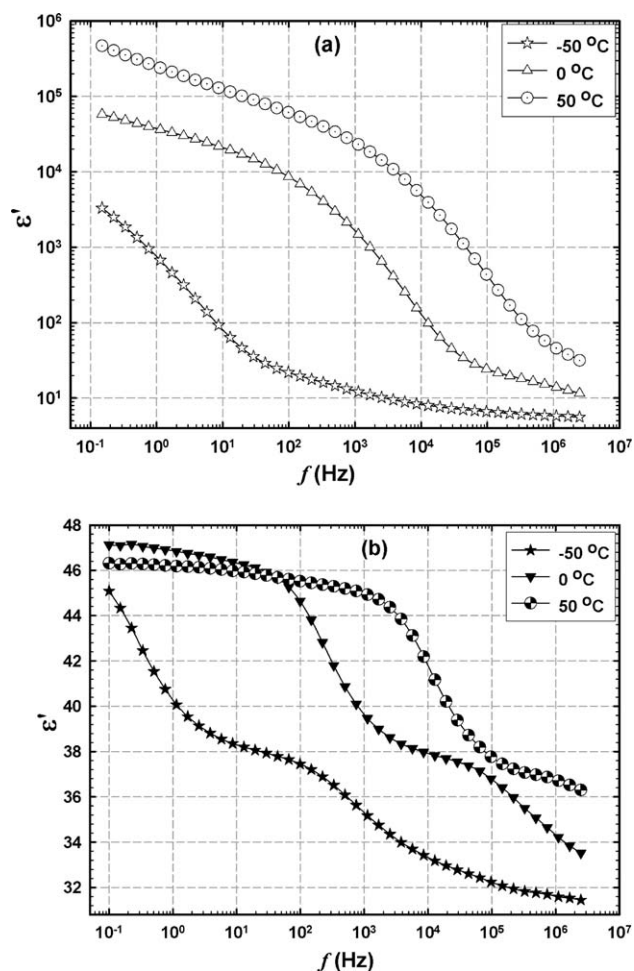
Figure 3. Frequency dependence of ε' for (a) $C_{60}(OH)_{29}$ and (b) $Sc_3N@C_{80}(OH)_{18}$ samples at three temperatures.
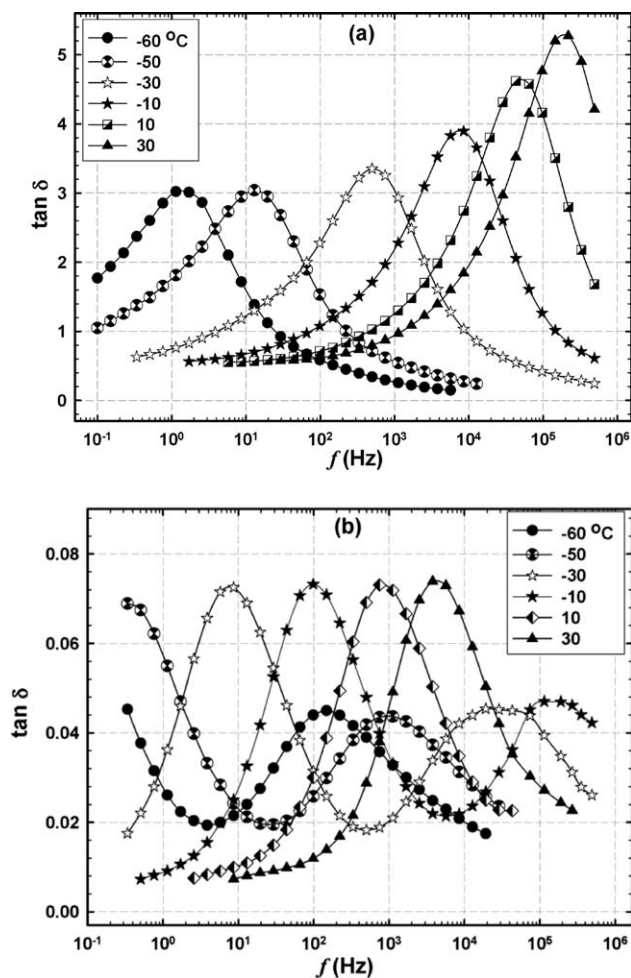
Figure 4. Tan δ versus frequency at select temperatures for (a) $C_{60}(OH)_{29}$ and (b) $Sc_3N@C_{80}(OH)_{18}$ samples.

dynamics of chain motions and associated relaxation differences among the fullerene samples explored over a broad temperature range.[41]

Whereas the previous discussion focused on the dielectric properties of the individual nanoparticles, C_{60}, $C_{60}(OH)_{29}$, $Sc_3N@C_{80}$, and $Sc_3N@C_{80}(OH)_{18}$, the following sections present the analysis for the PU networks incorporating them, C_{60}-PU and $Sc_3N@C_{80}$-PU. The effects of nanoparticle type (C_{60} vs. $Sc_3N@C_{80}$) and percent composition on ε' versus f profiles of fullerene–PU networks at 20°C are illustrated in Figure 5. The family of curves for $Sc_3N@C_{80}$-PU lie above the family for the C_{60}-PU networks and this enhanced response, similar to that observed for C_{60} versus $Sc_3N@C_{80}$ in the absence of a matrix, is attributed to the metallic nitride complex encapsulate. For both C_{60}-PU and $Sc_3N@C_{80}$-PU networks, the dielectric response increases as fullerene loading increases. In all cases, there are at least a theoretical equivalent of isocyanate groups in the synthesis of the polymer matrix, which should result in an increase in crosslinking and reduced number of dangling ends as the fullerenol concentration is increased. However, material characterization suggests that at higher fullerenol loadings, there remain a significant number of unreacted groups. One explanation for

the increase in dielectric response might involve an increase in polymer free volume v_f due to fullerene cages acting as polymer packing defects. A similar effect was observed by Lu et al. [22] in their studies of the dielectric properties of benzylaminofullerene (BAF)-polyethylene composites as a function of BAF loading. However, the study of dielectric properties of polyimide films with different C_{60} and C_{70} loadings as admixtures by Subocz et al.[42] demonstrated that as C_{60} or C_{70} concentration increases, the dielectric permittivity of the resultant films decreases due to restriction on polymer chain motions posed by these structures. A similar result was obtained by Ouyang et al.[43] who studied the effect of C_{60}-fullerenol density on the dielectric properties of C_{60}/poly(dimethylsiloxane) and found that at low fullerenol density the real permittivity of the composite decreases as fullerenol loading increases due to restriction of polymer chain motions to which dipole motions are coupled. However, at high density, the dielectric constant was seen to increase with increase in fullerenol loading due to polarizability arising from unreacted -OH groups in the composite. In the current study, an argument could be constructed for the increased free volume of an imperfect network as fullerene concentration increases and the increase in concentration of the more polarizable network component.

The temperature response of ε'' versus f at 1.0 Hz for PU networks at different fullerene loadings is shown in Figure 6. For $T < 0°C$, three relaxation features are seen for all networks. After 0°C, ε'' monotonically rises with increasing temperature, and there are no relaxation peaks in this region. In comparing the dielectric plots with the DMA results from Figure 1(b), the peaks at ca. $-50°C$ would correspond to the glass transition and those at $-130°C$ are due to short range chain motions in the glassy state. Support for the latter mechanism is that this relaxation appears the same regardless of the identity of the fullerene crosslinker. The weak feature at ~25°C corresponds to the dynamic mechanical feature, seen in Figure 1(a,b) that was associated with thermally-driven reactions between unreacted hydroxyl groups on $C_{60}(OH)_{29}$ and polymer end groups. The ε'' curve for the lowest crosslinking degree (0.8% C_{60}-PU) has the lowest ε'' values before T_g but becomes the highest for $T > T_g$.
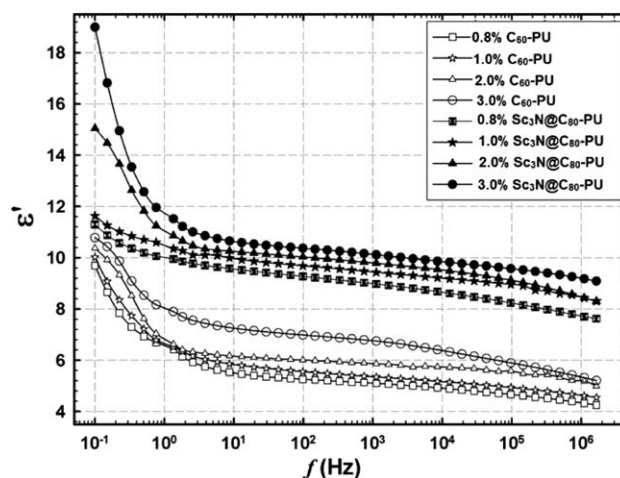
Figure 5. ε' versus f for fullerene–PU variants at 20°C.
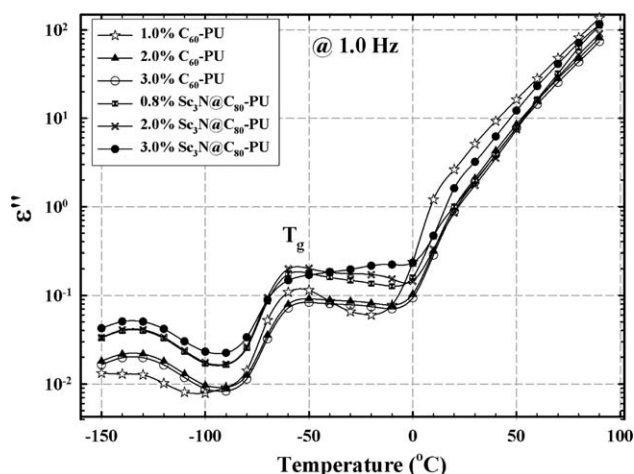
Figure 6. Temperature dependence of ε'' at 1.0 Hz for fullerene–PU variants.

Chiang et al.[44] showed a similar dynamic mechanical loss peak at around $-60°C$, as well as a DSC transition for a C_{60}-PU network.

ε' and ε'' were also determined for the prepared fullerene–PU networks using an alternate test assembly comprised of a Keithley 4200-SCS instrument and custom electrode assembly, as described in the Experimental section. This instrument allows for expanding the frequency range (10 KHz to 10 MHz) at room temperature. The frequency dependence of the permittivity of fullerene–PU networks measured using this instrument is provided in Figure 7(a). When compared to the results obtained using the Novocontrol broadband dielectric spectrometer shown in Figure 5, excellent correlation exists within the same frequency range. Up to 3 MHz, ε' of all samples decreases with increasing frequency, because, as before, at higher frequencies the characteristic dipole reorientation times are increasingly too slow to remain in step with the applied electric field oscillations. After 3 MHz, ε' increases again with increasing frequency, which is not classical behavior, and, at present, is not understood. Similar behavior is seen in Figure 7(b), which illustrates ε'' versus frequency for fullerene–PU network variants.

An interesting observation is the higher values of ε' over ε'', suggesting that nanocomposites constructed in this way, and using these materials, may ultimately be desirable for use in electronics applications, such as energy storage media.[45] Since the maximum electrical energy storage capacity (U_{max}) of a linear dielectric material is given by $U_{max} = \varepsilon' \, E_b^2/2$ where E_b is the dielectric breakdown strength (DBS), both large ε' and high DBS are required for large electric energy storage.[45–49] Consequently, incorporating materials with large ε' within polymeric matrices of high DBS and possessing excellent mechanical properties might lead to a large energy storage dielectric material.[45,47,48] Of particular significance with regard to this application is the fact that the real permittivity of the neat sample is lower than that of the $Sc_3N@C_{80}$-PU nanocomposite, as seen in Figure 8. A similar indicator regarding future potential of these nanocomposites as energy storage systems can be observed in Figure 8, which
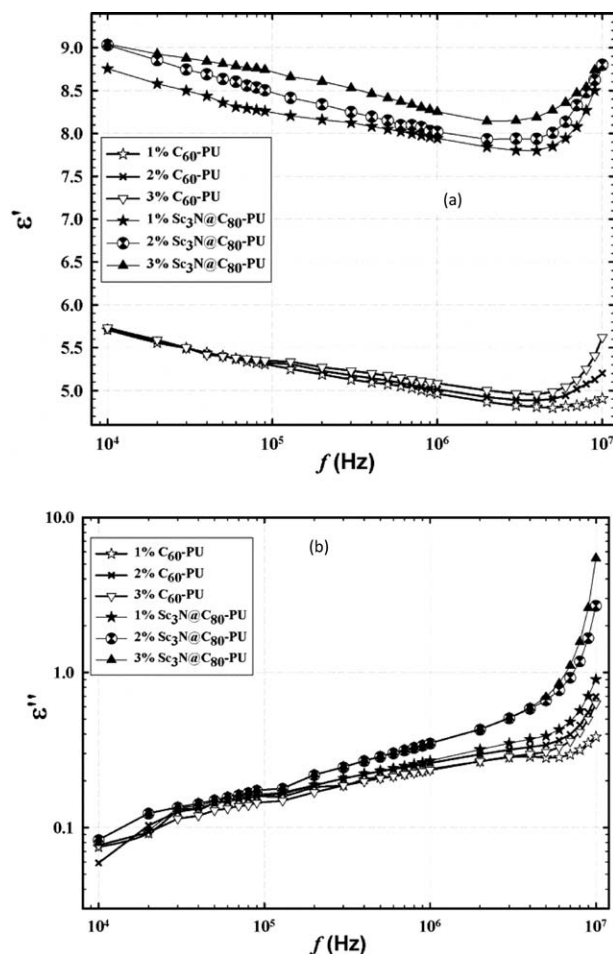
Figure 7. (a) ε' and (b) ε'' versus f for fullerene–PU variants at 22°C (data via Keithley 4200-SCS).

illustrates the high ε' relative to ε'' values for $Sc_3N@C_{80}$ and 3% $Sc_3N@C_{80}$-PU—versus that of the neat linear PU control—as determined by the BDS at 20°C.
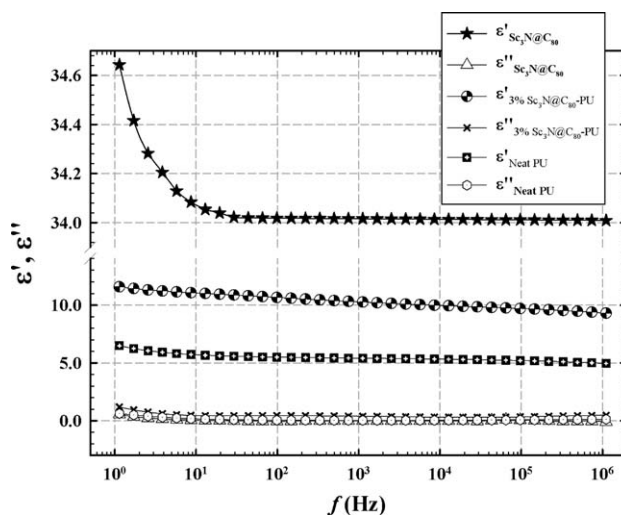
Figure 8. ε' and ε'' versus f for $Sc_3N@C_{80}$ and 3% $Sc_3N@C_{80}$-PU versus Neat PU networks at 20°C (data via Novocontrol BDS).
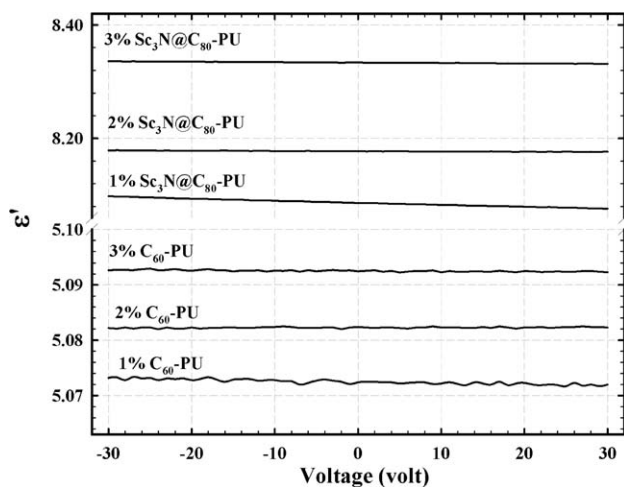
Figure 9. ε' versus applied dc bias voltage, at 1 MHz, and at 22°C for fullerene–PU networks (data via Keithley 4200-SCS).

The permittivity versus applied dc voltage measurement is a technique used for characterization of semiconductor materials and devices by varying the applied dc voltage and recording the response as a change in the capacitance. The fundamental nature of these measurements makes them useful in a wide range of applications since they are used to evaluate new materials, processes, devices, and circuits.[50] The real permittivity versus applied DC bias voltage for fullerene–PU samples collected at a frequency of 1 MHz using the Keithley 4200-SCS instrument and custom electrode assembly is provided in Figure 9. For all samples and within the available voltage range, there is a linear dielectric response in variation of the applied voltage, especially at low loading of fullerene.

Surface and volume resistivities of the fullerene–PU samples are presented in Table II and Figure 10. Volume resistivity is measured by applying a voltage across the sample, ranging from -210 to $+210$ v, and measuring the resulting current. In contrast, the surface resistivity is measured by applying a voltage across the surface of the sample as described in the Experimental section. The surface and volume resistivities at two different relative humidities, RH (1 and 20%) are listed in Table II.

Resistivity results might indicate subtle dependence on RH and concentration of fullerene additive. The volume resistivities of the $Sc_3N@C_{80}$-PU samples are lower than those of the C_{60}
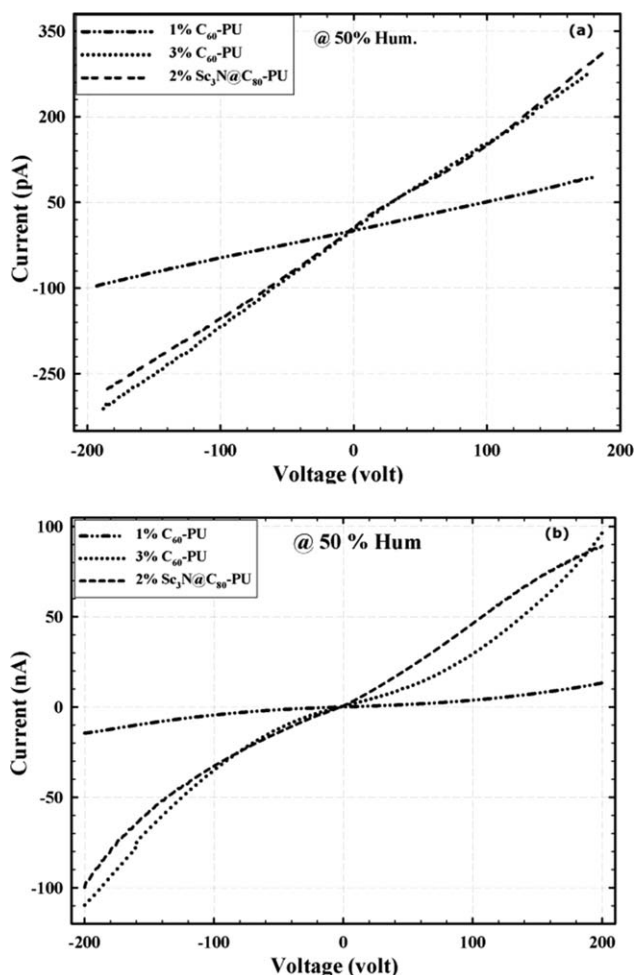
Figure 10. Current–voltage characteristics of fullerene–PU samples at 50% RH; (a) surface resistivity (σ) and (b) volume resistivity (ρ) is calculated from the slopes of the plots (data via Keithley 4200-SCS).

analogs by an order of magnitude. Perhaps, this is due to the presence of the metal-nitride cluster, Sc_3N, altering fullerene cage partial charge distribution that, in turn, interacts with sorbed water molecules.[1–4] Overall, the volume resistivity of prepared fullerene networks lies between 10^{12} and 10^{14} Ω cm. For reference, polymers with volume resistivity ranging from 10^{15} to 10^{22} Ω cm are considered good insulators.[51] Since an RH effect attributed to sorbed water is suggested by Table II,

Table II. Surface and Volume Resistivities of Fullerene–PU Samples at Different Fullerene Loadings and RH

Sample Humidity	Surface resistivity (Ω)		Volume resistivity (Ω cm)	
	1%	20%	1%	20%
1% C_{60}-PU	1.9E+13	1.6E+13	4.4E+14	2.4E+14
2% C_{60}-PU	2.0E+13	1.5E+13	3.0E+14	2.6E+14
3% C_{60}-PU	1.8E+13	1.0E+13	1.4E+14	5.6E+13
1% $Sc_3N@C_{80}$-PU	1.8E+13	1.6E+13	5.6E+13	4.1E+13
2% $Sc_3N@C_{80}$-PU	1.8E+13	1.7E+13	4.9E+13	3.7E+13
3% $Sc_3N@C_{80}$-PU	1.8E+13	1.69E+13	1.9E+13	3.5E+13

the resistivity of three samples was measured at the higher RH of 50% RH and the current–voltage profiles of these samples are presented in Figure 10. The observed nonlinearity for the volume current–voltage curves can be associated with two factors in a general sense: conduction mechanism and sorbed humidity. Surface and volume resistivities at 50% RH for these three samples are as follows: 1%C60-PU: 1.1E+14 Ω and 5.7E+13 Ω cm; 3%C_{60}-PU: 3.3E+13 Ω and 7.2E+12 Ω cm; 2%Sc3N@C80-PU: 3.3E+13 Ω and 6.1E+12 Ω cm. Increasing RH from 1 to 50% may lead to a 2 order-of-magnitude decrease in resistivity so that charge hopping along hydrogen bonded water molecules might be considered.

CONCLUSIONS

Fullerene–polymer nanocomposites comprising PU macromolecules end-linked by polyhydroxylated fullerenes (C_{60} and $Sc_3N@C_{80}$) were prepared via polyaddition reactions between the hydroxyl groups on the fullerene cages and the NCO groups of a diisocyanate prepolymer. Gel fractions of the resulting fullerene–PU networks are high, ranging from 72 to 97% and thermal stabilities are considerable based on TGA degradation onset temperatures up to 300°C.

Dynamic mechanical analyses of fullerene–PU networks indicate a glassy material at low temperatures and rubbery material at high temperatures, with T_g around −50°C. A sub-T_g transition in the range of −150 to −110°C is ascribed to local crankshaft motions in the methylene sections of the chains. BDS also uncovered a relaxation in the loss spectrum in the range of −150 to −110°C for all samples. This relaxation is assigned to local motions along the PU chains that are not influenced by crosslinks or the presence of the Sc_3N encapsulate. In harmony with the dynamic mechanical spectral assignment in this region, these motions are also attributed to crankshaft motions in the methylene sections. Above T_g there is a high temperature feature that is likely due to thermally driven crosslinking reactions during analysis. These postreactions must be taken into consideration when processing these nanocomposite materials in future applications.

BDS examination of free fullerenes (C_{60}, $C_{60}(OH)_{29}$, $Sc_3N@C_{80}$, $Sc_3N@C_{80}(OH)_{18}$) revealed large ε' values for the hydroxylated fullerene analogs attributed to the large number of attached polar OH dipoles. Two relaxations for $Sc_3N@C_{80}(OH)_{18}$ were identified and are suggested to arise from (1) reorientation of hydroxylated cages and (2) reorientations within encapsulated Sc_3N complexes.

ε' Values of $Sc_3N@C_{80}$-PU are larger than those of C_{60}-PU at a given frequency and rather high at low frequencies.

Surface and bulk resistivities of fullerene–PU networks were measured and found to be dependent on relative humidity. Materials respond with a relatively constant linear capacitance, that is, constant real permittivity, over a varied applied dc bias of −30 to +30 volts.

A general conclusion that can be drawn from these overall results is that this class of materials can be rendered quite polarizable and the fact that ε' is considerably greater than ε'' suggests that they may prove useful as high-energy dielectric storage media for high capacitance applications.

REFERENCES

1. Suzuki, T.; Maruyama, Y.; Kato, T.; Kikuchi, K.; Achiba, Y. *J. Am. Chem. Soc.* **1993**, *115*, 11006.

2. Yamamoto, K.; Funasaka, H.; Takahashi, T.; Akasaka, T. *J. Phys. Chem.* **1994**, *98*, 12831.

3. Akasaka, T.; Okubo, S.; Kondo, M.; Maeda, Y.; Wakahara, T.; Kato, T.; Suzuki, T.; Yamamoto, K.; Kobayashi, K.; Nagase, S. *Chem. Phys. Lett.* **2000**, *319*, 153.

4. Anderson, M. R.; Dorn, H. C.; Stevenson, S. A. *Carbon* **2000**, *38*, 1663.

5. Stevenson, S.; Mackey, M. A.; Coumbe, C. E.; Phillips, J. P.; Elliott, B.; Echegoyen, L. *J. Am. Chem. Soc.* **2007**, *129*, 6072.

6. Stevenson, S.; Harich, K.; Yu, H.; Stephen, R. R.; Heaps, D.; Coumbe, C. E.; Phillips, J. P. *J. Am. Chem. Soc.* **2006**, *128*, 8829.

7. Liu, S.; Sun, S. *J. Organomet. Chem.* **2000**, *599*, 74.

8. Dunsch, L.; Yang, S. *Electrochem. Soc. Interface* **2006**, *15*, 34.

9. Akasaka, T.; Nagase, S. Endofullerene: a New Family of Carbon Clusters; Kluwer Academic Publishers: Dordrecht, **2002**.

10. Guha, S.; Nkamoto, K. *Coord. Chem. Rev.* **2005**, *249*, 1111.

11. Chaur, M. N.; Frederic, M.; Bevan, E.; Andreas, A. J.; Kenneth, W.; Brian, H. C.; Luis, E. *J. Am. Chem. Soc.* **2007**, *129*, 14826.

12. Chaur, M. N.; Athans, A. J.; Echegoyen, L. *Tetrahedron* **2008**, *66*, 11387.

13. Fatouros, P. P.; Corwin, F. D.; Chen, Z.; Broaddus, W. C.; Tatum, J. L.; Kettenmann, B.; Ge, Z.; Gibson, H. W.; Russ, J. L.; Leonard, A. P.; Duchamp, J. C.; Dorn, H. C. *Radiology* **2006**, *240*, 756.

14. Zhang, J.; Fatouros, P. P.; Shu, C.; Reid, J.; Owens, L. S.; Cai, T.; Gibson, H. W.; Long, G. L.; Corwin, F. D.; Chen, Z.; Dorn, H. C. *Bioconjugate Chem.* **2010**, *21*, 610.

15. Bethune, D. S.; Johnson, R. D.; Salem, J. R.; de Vries, M. S.; Yannoni, C. S. *Nature* **1993**, *366*, 123.

16. Giacalone, F.; Martin, N. *Chem. Rev.* **2006**, *106*, 5136.

17. Badamshina, E. R.; Gafurova, M. P. *Polym. Sci. Ser. B* **2007**, *49*, 182.

18. Wang, C.; Guo, Z. X.; Fu, S.; Wu, W.; Zhu, D. *Prog. Polym. Sci.* **2004**, *29*, 1079.

19. Chiang, Y.; Wang, L. Y. *Trends Polym. Sci.* **1996**, *4*, 298.

20. Hawker, C. J. *Macromolecules* **1994**, *27*, 4836.

21. Pasimeni, L.; Franco, L.; Ruzzi, M.; Mucci, A.; Schenetti, L.; Luo, C.; Guldi, D. M.; Kordatos, K.; Prato, M. *J. Mater. Chem.* **2001**, *11*, 981.

22. Lu, Z.; He, C.; Chung, T. S. *Polymer* **2001**, *42*, 5233.

23. Wu, Y.; Fan, L.; Yang, S. *J. Phys. Chem. B* **2005**, *109*, 17831.

24. Fujn, A.; Umeda, T.; Shirakawa, T.; Akasaka, T.; Yoshino, K. *Jpn. J. Appl. Phys.* **2002**, *41*, 2254.

25. McCluskey, D. M.; Smith, T. N.; Madasu, P. K.; Coumbe, C. E.; Mackey, M. A.; Fulmer, P. A.; Wynne, J. H.; Stevenson, S.; Phillips, J. P. *ACS Appl. Mater. Interfaces* **2009**, *1*, 882.

26. Kremer, F.; Schönhals, A. Broadband Dielectric Spectroscopy; Springer: Berlin, **2003**; p 225.

27. Havriliak, S.; Negami, S. *J. Polym. Sci. Polym. Symp.* **1966**, *14*, 99.

28. Iwasa, Y.; Nuttall, C. J. *Synth. Met.* **2003**, *135–136*, 773.

29. Raw characterization data are provided in Supporting Information section.

30. Wang, S.; He, P.; Zhang, J.; Hiang, H. *Synth. Commun.* **2005**, *35*, 1803.

31. Wang, X. Thesis, Virginia Polytechnic Institute and State University, Blacksburg, **2006**.

32. Yannoni, C. S.; Hoinkis, M.; Vries, M. S.; Bethune, D. S.; Salem, J. R.; Crowder, M. S.; Johnson, R. D. *Science* **1992**, *256*, 1191.

33. Iezzi, E. B.; Cromer, F.; Stevenson, J. P.; Dorn, H. C. *Synth. Met.* **2002**, *128*, 289.

34. Velankar, S.; Cooper, S. L. *Macromolecules* **1998**, *31*, 9181.

35. Fragiadakis, D.; Runt, J. *Macromolecules* **2013**, *46*, 4184.

36. Wang, C. B.; Cooper, S. L. *Macromolecules* **1983**, *16*, 775.

37. Miller, J. A.; Lin, S. B.; Hwang, K. K. S.; Wu, K. S.; Gibson, P. E.; Cooper, S. L. *Macromolecules* **1985**, *18*, 32.

38. Su, J. S.; Chen, Y. F.; Chiu, K. C. *Appl. phys. Lett.* **1999**, *74*, 439.

39. Su, J. S.; Chen, Y. F.; Chiu, K. C. *Appl. Phys. Lett.* **1999**, *74*, 1607.

40. Sundqvist, B.; Persson, N. *J. Phys.: Condens. Matter* **2002**, *14*, 10437.

41. Ahmed, H. M.; Hassan, M. K.; Mauritz, K. A.; Buchanan, J. P. (in preparation).

42. Subocz, J.; Valozhyn, A.; Zenker, M. *Rev. Adv. Mater. Sci.* **2007**, *14*, 193.

43. Ouyang, J.; Zhou, S.; Wang, F.; Goh, S. H. *J. Phys. Chem. B* **2004**, *108*, 5937.

44. Chiang, L. Y.; Wang, L. Y.; Kuo, C. S. *Macromolecules* **1995**, *28*, 7574.

45. Siddabattuni, S.; Schuman, T. P.; Dogan, F. *Polym. Preprints* **2011**, *52*, 45.

46. Siddabattuni, S.; Schuman, T. P.; Dogan, F. *Polym. Preprints* **2011**, *52*, 92.

47. Xiaojun, Y.; Zhimin, Y.; Changhui, M.; Jun, D. *Rare Metals* **2006**, *25*, 250.

48. Li, J. Y.; Zhang, L.; Ducharme, S. *Appl. Phys. Lett.* **2007**, *90*, 132901.

49. Doi, M.; Edward, S. F. The Theory of Polymer Dynamics; Oxford University Press: New York, **1986**.

50. Stauffer, L. Keithley Instruments, Inc., Fundamentals of Semiconductor C-V Measurements, **2009**.

51. Brydson, J. A. Plastic Materials, 5th ed.; Butterworth: Boston, **1990**.